Predictability of summer Northwest Pacific Climate in Eleven Coupled Model Hindcasts: Local and remote forcing

J. S. Chowdary, Shang-Ping Xie, June-Yi Lee, Yu Kosaka and Bin Wang

International Pacific Research Center, University of Hawaii at Manoa, Honolulu, Hawaii.

APCS(APEC Climate Symposium)
June-20-24, 2010
Busan, Korea

Objective: To assess the predictability of Northwest (NW) Pacific climate variability in summer following El Niño in the eleven-model ensemble, and to investigate role of local and remote forcing in predicting NW Pacific atmospheric anomalies.

Background:

✓**Boreal summer (JJA) is the major rainy season for East Asia, and prediction of summer rainfall is of great socio-economic value to this region.**

✓**Summer rainfall variability in subtropical/mid-latitude (20°-40°N) East Asia is tied to the westward extension of the subtropical high (anticyclone) in the Northwest (NW) Pacific (10°-30°N) (Huang et al. 2004), both in turn correlate with the El Niño-Southern Oscillation (ENSO) (Zhang et al. 1996; Harrison and Larkin 1996; Wang et al. 2000, 2003). The great flood in the summer of 1998 in the Yangtze River Valley is an example.**

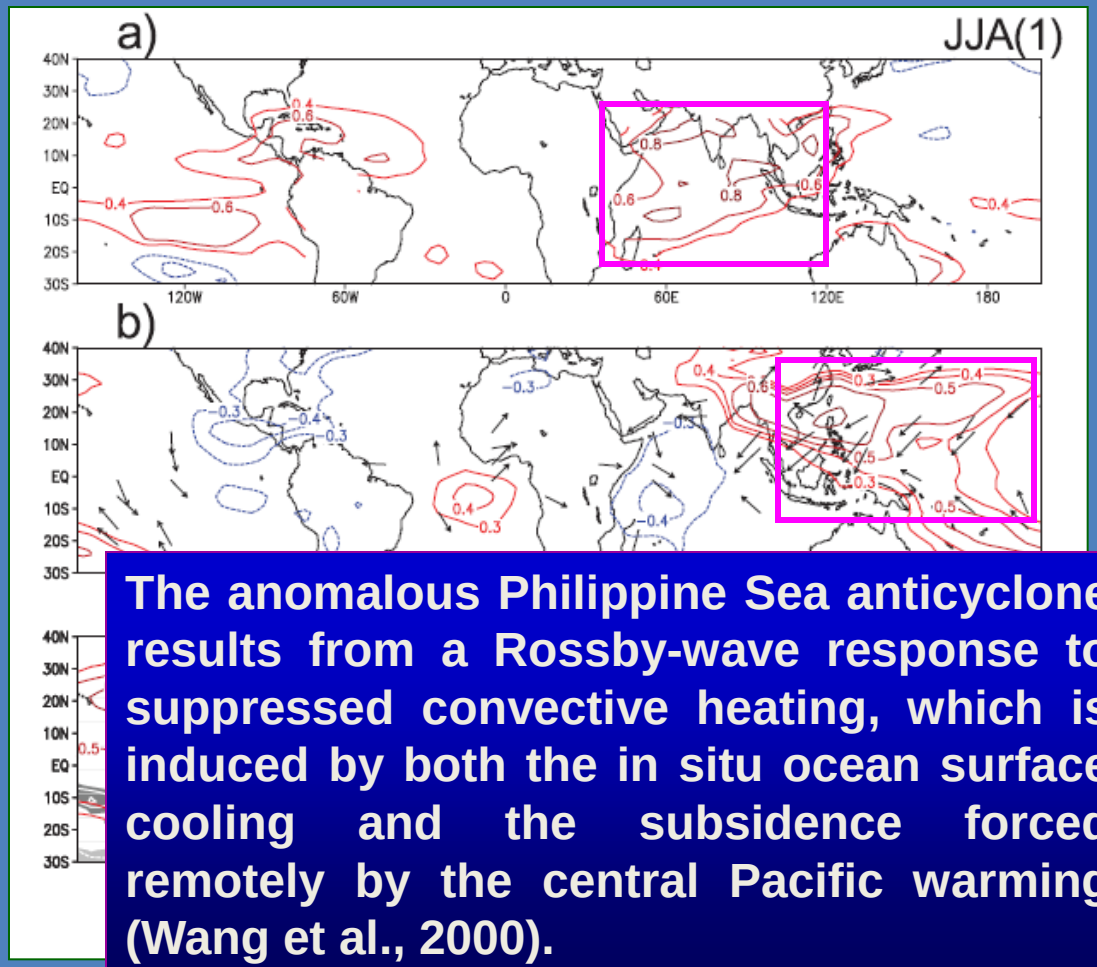

SST

SLP & Winds

Rainfall & TT

The anomalous Philippine Sea anticyclone results from a Rossby-wave response to suppressed convective heating, which is induced by both the in situ ocean surface cooling and the subsidence forced remotely by the central Pacific warming (Wang et al., 2000).

JJA(1) correlation with NDJ(0/1) Nino-3.4 SST Index (Xie at al., 2009)

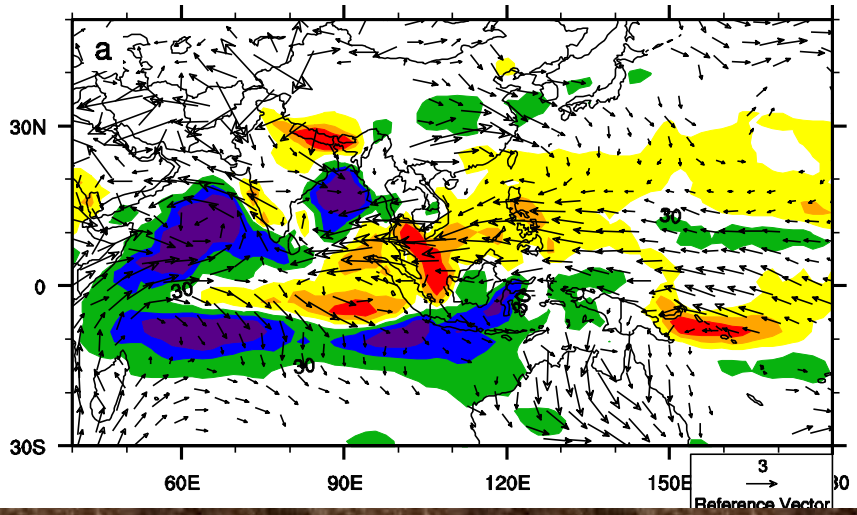

JJA

Huang et al (2010)

(ECHAM5.3)

Difference of mean summer precipitation (color-shaded) and 850hpa wind (a) between all tropical Indian Ocean SST add1k experiment and climatological SST experiment.

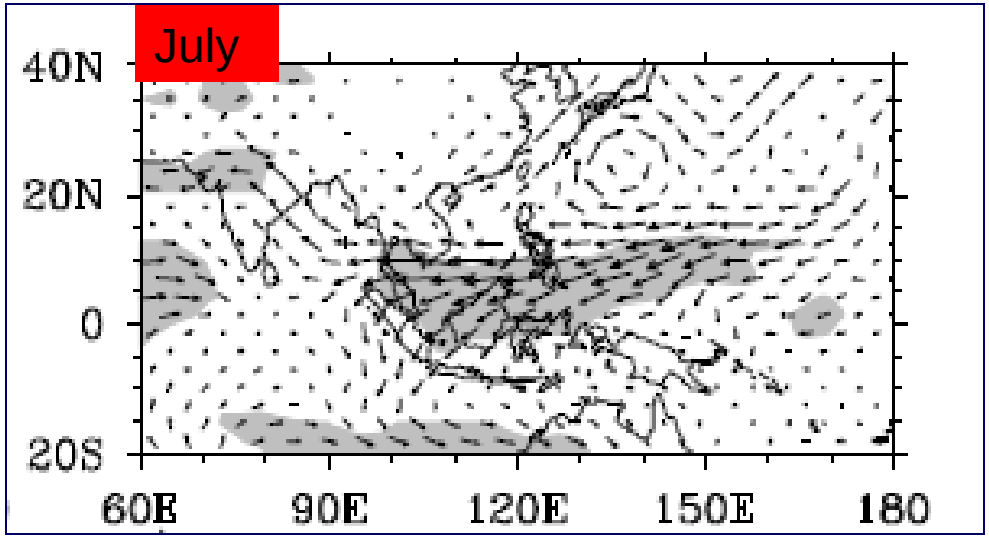

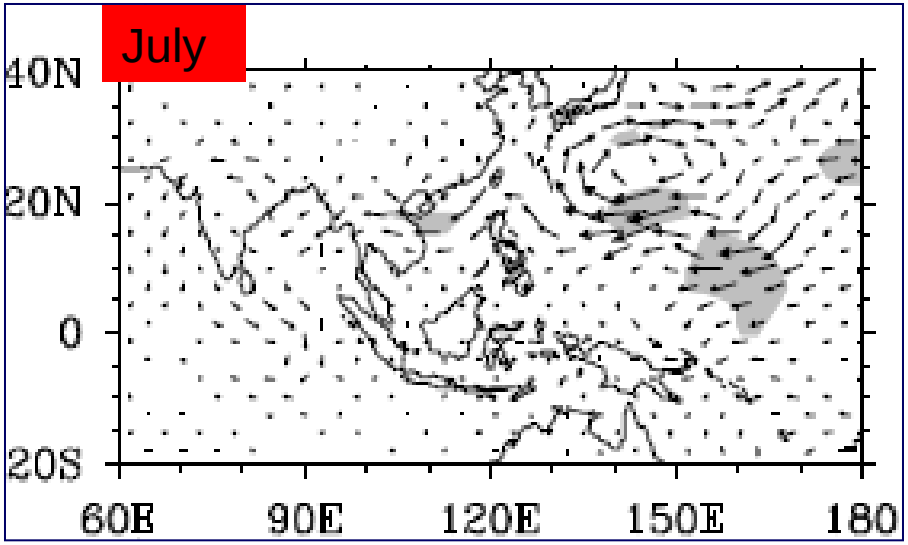

Fig. Difference of 850hPa wind (units: m/s) between (a) the TIO and CTRL runs and NW Pacific and CTRL runs. ECHAM4. Wu et al (2010).

Data:

➢**The hindcast data set is derived from 11 global coupled ocean-atmospheric general circulation models (CGCMs). They include seven coupled models from the European Center's Development of a European Multi-Model Ensemble System for Seasonal to Inter-Annual Prediction (DEMETER) database (Palmer et al. 2004) and four coupled models from the Asian-Pacific Economic Cooperation Climate Center (APCC)/Climate Prediction and its Application to Society (CliPAS) project [Wang et al., 2009].**

➢**Model results are compared with: HadISST data [*Rayner et al*., 2003], NCEP reanalysis 2 [*Kanamitsu et al*., 2002] for SLP, geopotential height and winds at the 850 and 200 hPa levels and CMAP precipitation [*Xie and Arkin*, 1996].**

➢**Various statistical methods are used such as empirical orthogonal function (EOF), correlation, regression and composites to evaluate model skills and to determine the physical mechanisms.**

Details of Models: Analysis period is form 1980 to 2001 : MME is for 1982 to 2001

Abbreviation	Institute	AGCM	OGCM	Ensemble number and period	Reference
BMRC	BMRC-POAMA1.5	BAM 3.0d T47 L17	ACOM2 0.5–1.5°lat 2°lon L31	10; 1980–2002	Zhong et al. (2005)
CERF	CERFACS	ARPEGE T63L31	OPA 8.2 2° lat 2°lon L31	9;1980-2001	Palmer et al. (2004)
ECMW	ECMWF	IFS T95L40	HOPE-E 0.3-1.4° lat 1.4°lon L29	9;1980-2001	Palmer et al. (2004)
GFT1	GFDL	AM2.1 2°lat 2.5°lon L24	OM3.1 (MOM4) 1/3°lat 1°lon L50	10; 1979–2005	Delworth et al. (2006)
INGV	INGV	ECHAM4 T42L19	OPA8.1 0.5–1.5°lat 2°lon L31	9;1980-2001	Palmer et al. (2004)
LODY	LODYC	IFS T95L40	OPA8.2 2° lat 2°lon L31	9;1980-2001	Palmer et al. (2004)
METF	Météo-France	ARPEGE T63L31	OPA 8.0 182 GP × 152 GP L31	9;1980-2001	Palmer et al. (2004)
MAXP	MPI	ECHAM-5 T42L19	MPI-OM1 0.5–2.5°lat 2.5°lon L23	9;1980-2001	Palmer et al. (2004)
NCEP	NCEP	CFS T62 L64	MOM3 1/3°lat 1°lon L40	15; 1981–2004	Saha et al. (2006)
SINT	FRCGC- SINTEX-F	ECHAM4 T106 L19	OPA 8.2 2°cos(lat) 2°lon L31	9; 1982–2004	Luo et al. (2005)
UKMO	Met Office	HadAM3 2°lat 3.75°lon L19	GloSeaOGCM 0.3–1.25°lat 1.25°lon L40	9; 1980–2001	Palmer et al. (2004)

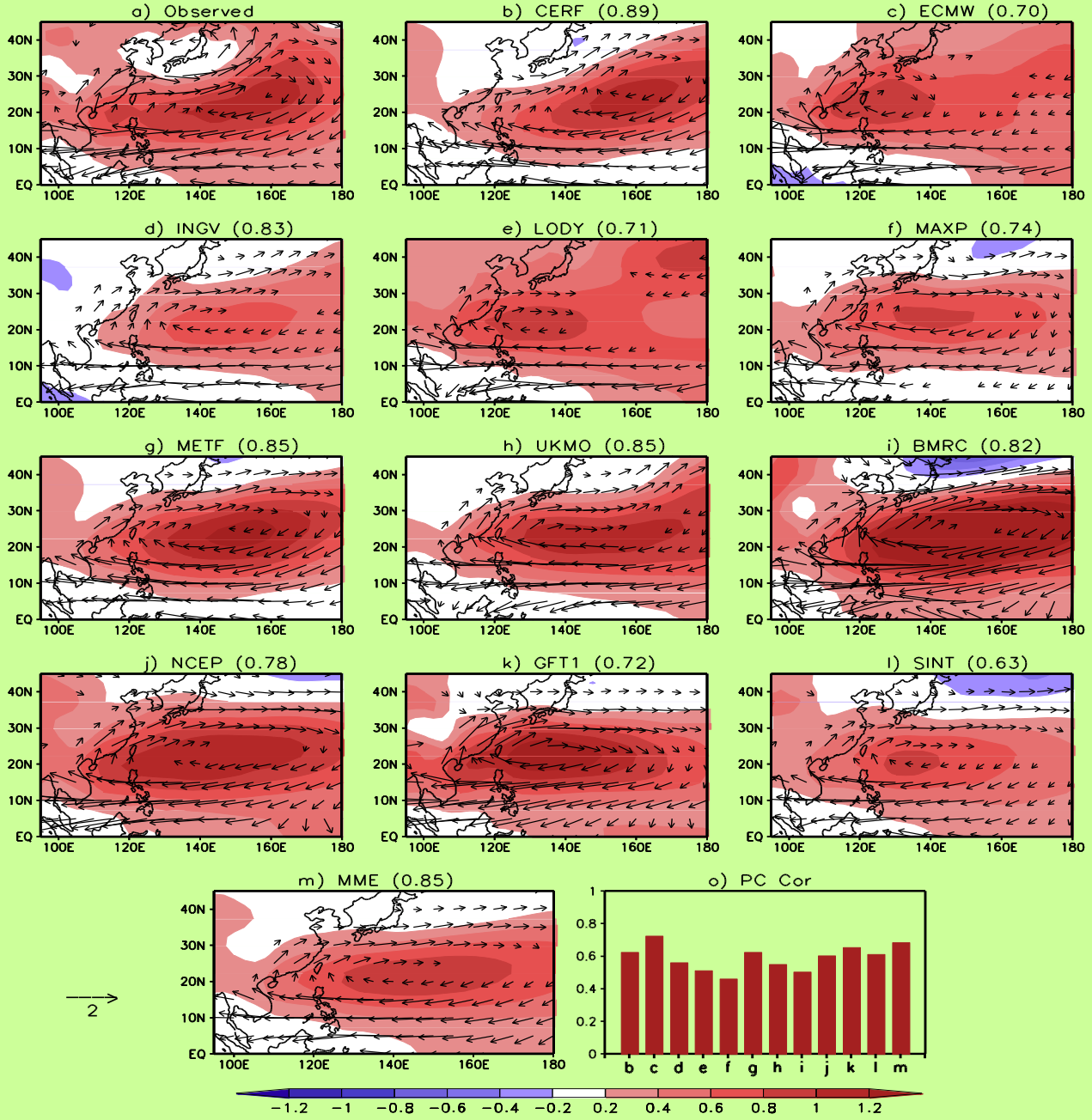
a) Observed
b) CERF (0.89)
c) ECMW (0.70)
d) INGV (0.83)
e) LODY (0.71)
f) MAXP (0.74)
g) METF (0.85)
h) UKMO (0.85)
i) BMRC (0.82)
j) NCEP (0.78)
k) GFT1 (0.72)
l) SINT (0.63)
m) MME (0.85)
o) PC Cor
40N
30N
20N
10N
EQ
100E
120E
140E
160E
180
2
0
0.2
0.4
0.6
0.8
1
b c d e f g h i j k l m
−1.2 −1 −0.8 −0.6 −0.4 −0.2 0.2 0.4 0.6 0.8 1 1.2

Rainfall EOF-2

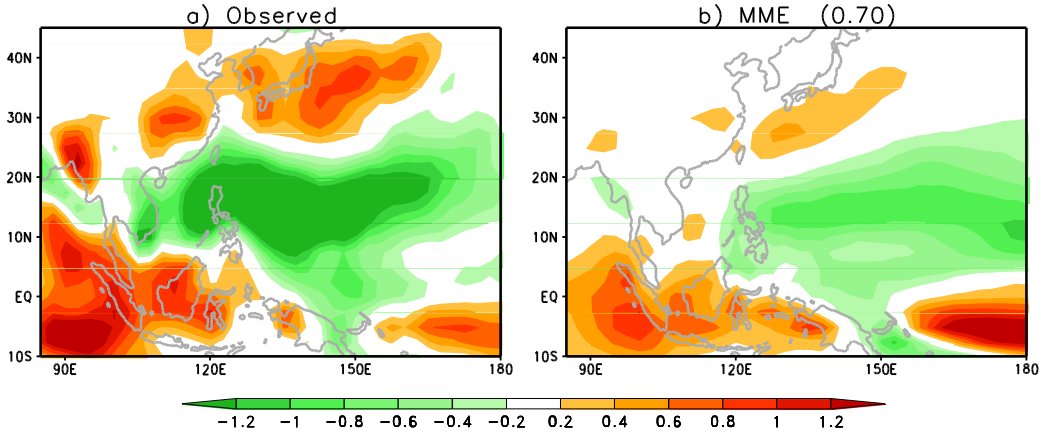

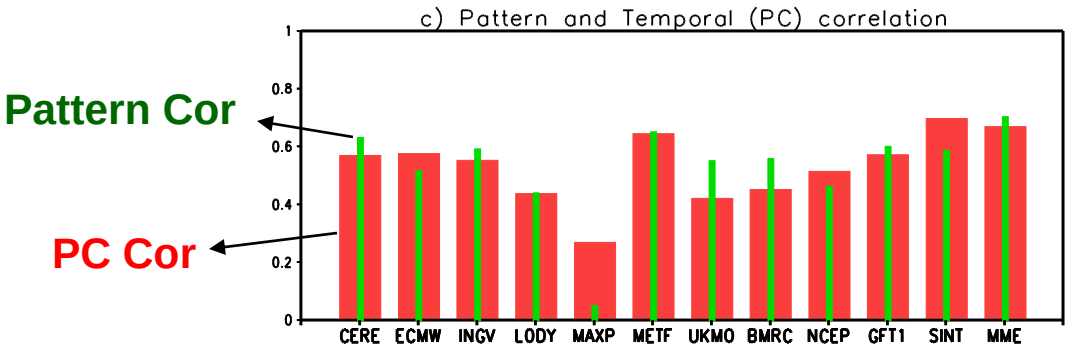

The second EOF of JJA rainfall anomalies (hPa) obtained from (a) observations and (b) MME. (c) Pattern (green) Temporal (red) correlation in PC between observations and each model.

✓In comparison with observations, there is a southward displacement of positive rainfall anomalies over the Japan in most models.

✓Except MAXP, all models displayed reasonable skills in predicting the JJA(1) rainfall over the NW Pacific at one-month lead. Temporal correlation of PC also exceeds 0.43 in most models, significant at 95% confidence level.

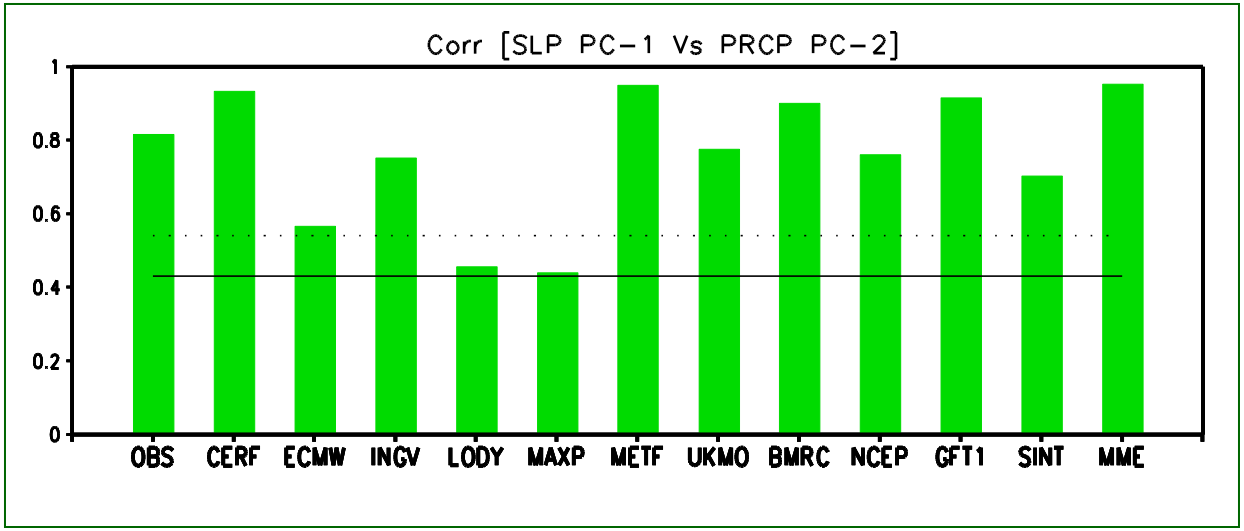

Correlation between the NW Pacific SLP PC-1 and precipitation PC-2 for observations, individual models and MME based on one-month lead prediction. Solid and dotted lines represent 95% and 99% confident levels, respectively.

✓Correlation coefficient between the first SLP PC and the second rainfall PC is 0.8 for observations and 0.95 for the MME prediction.

✓Some models (LODC, and MAXP) far underestimate the relationship. These models tend to have low skills for the second rainfall PC.

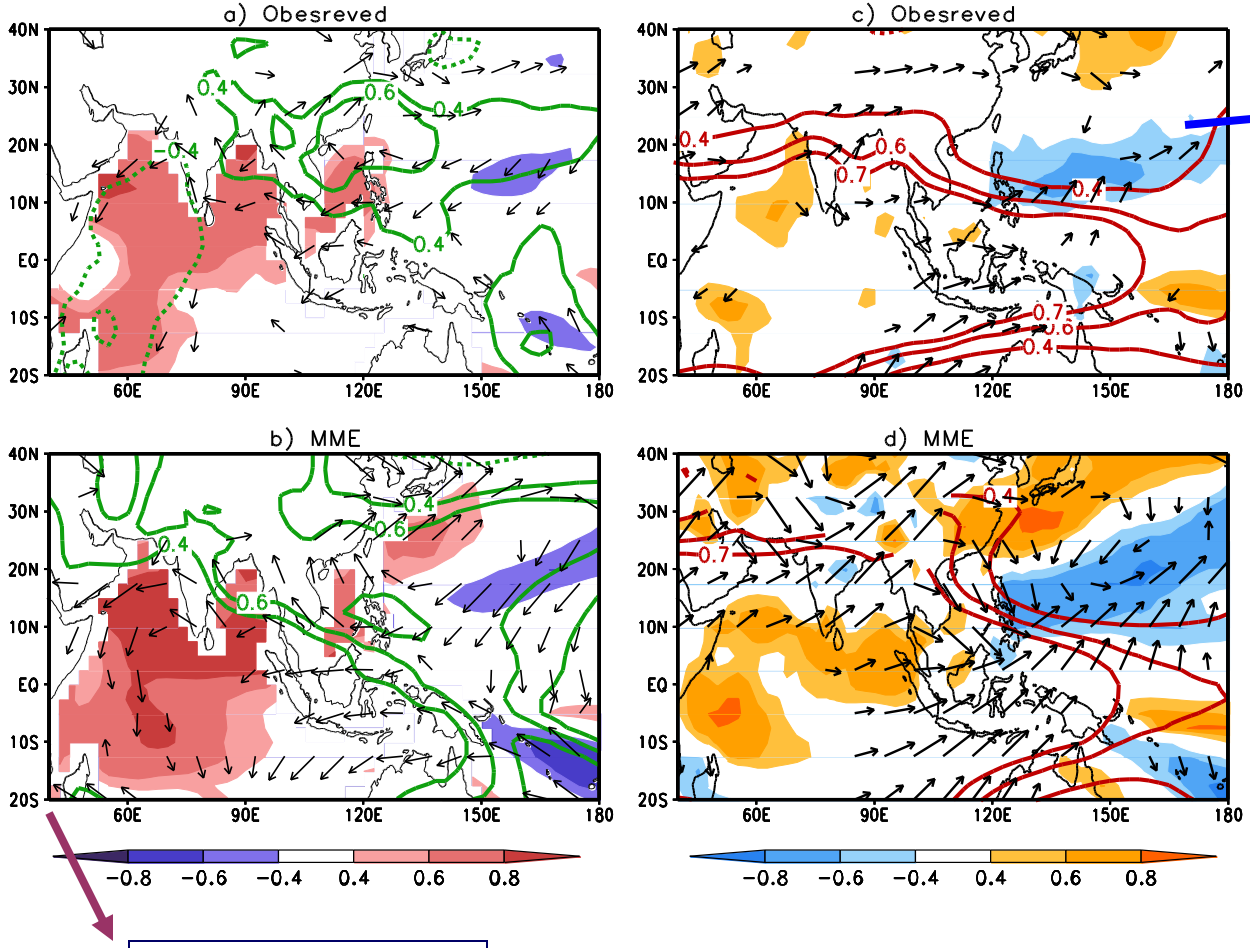

Rainfall (shaded)
TT (contour)
200hpa winds

NDJ(0) Niño-3.4 SST index correlation with JJA(1).

SST (shaded)
SLP (contour)
850hpa winds

ENSO-Teleconnections are well represented in MME one-month lead prediction.

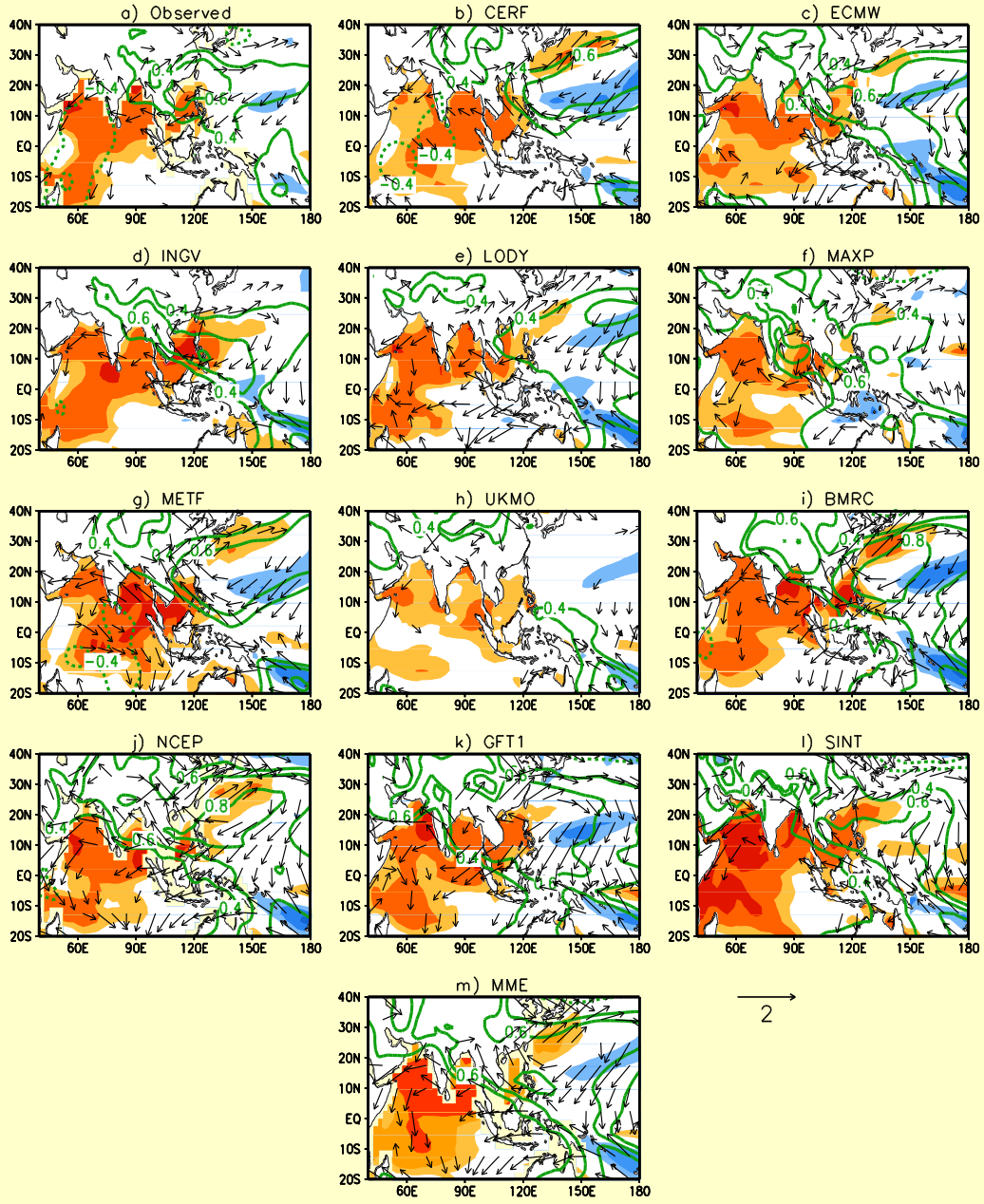

✓Most models capture positive SST correlations over the western and northern Indian Ocean (NIO), consistent with observations.

✓Many models reproduce the SLP correlation distribution over the NW Pacific in one-month lead prediction.

✓A few models failed to predict the weak negative SST anomaly over NW Pacific.

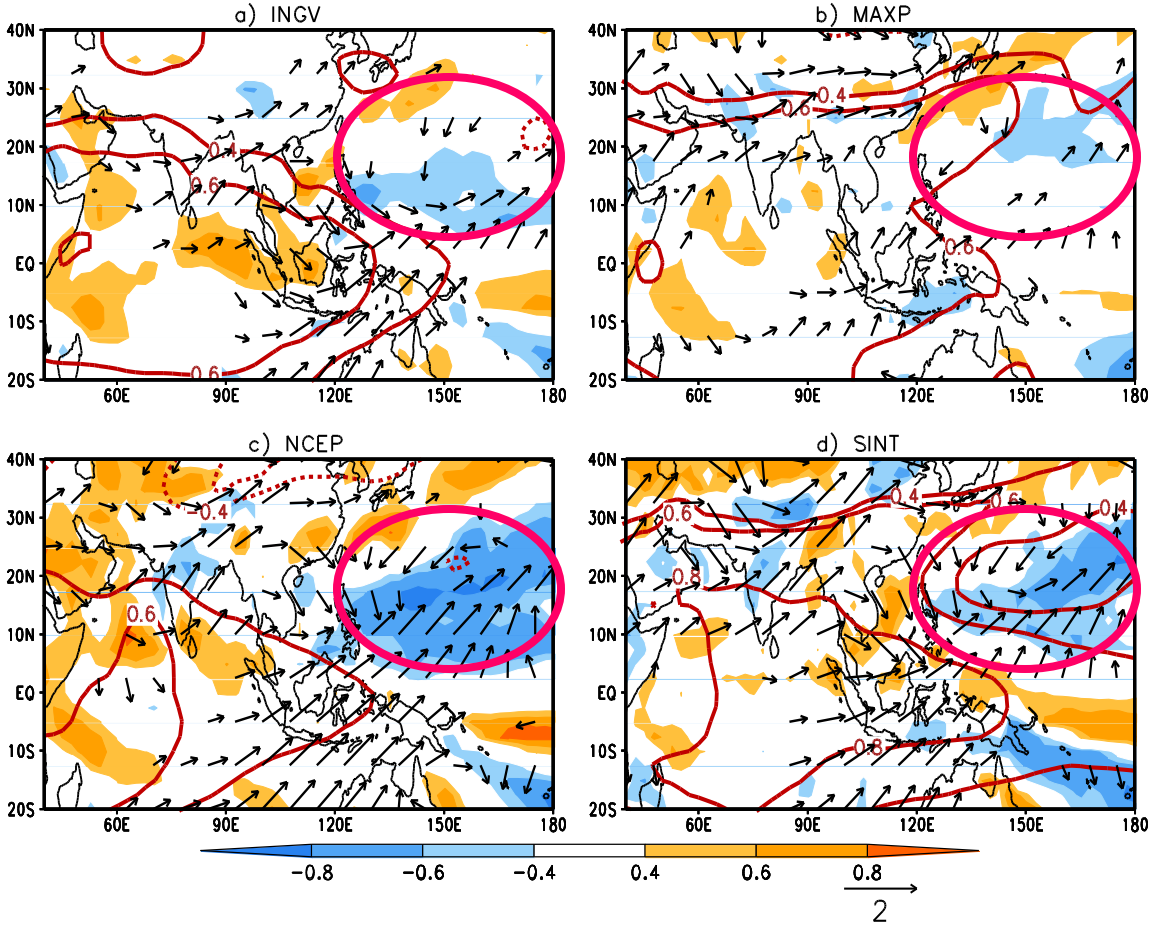

NDJ(0) Niño-3.4 SST index correlation with JJA(1) precipitation (shaded), tropospheric temperature (contours) and 200hPa wind velocity (vectors)

✓All models show the negative correlation of precipitation over the southeast flank of the 850 hPa anticyclonic anomalies in the NW Pacific in JJA(1).

✓Upper level (200hPa) winds and TT show significant variations over the Indo-western Pacific during JJA(1)

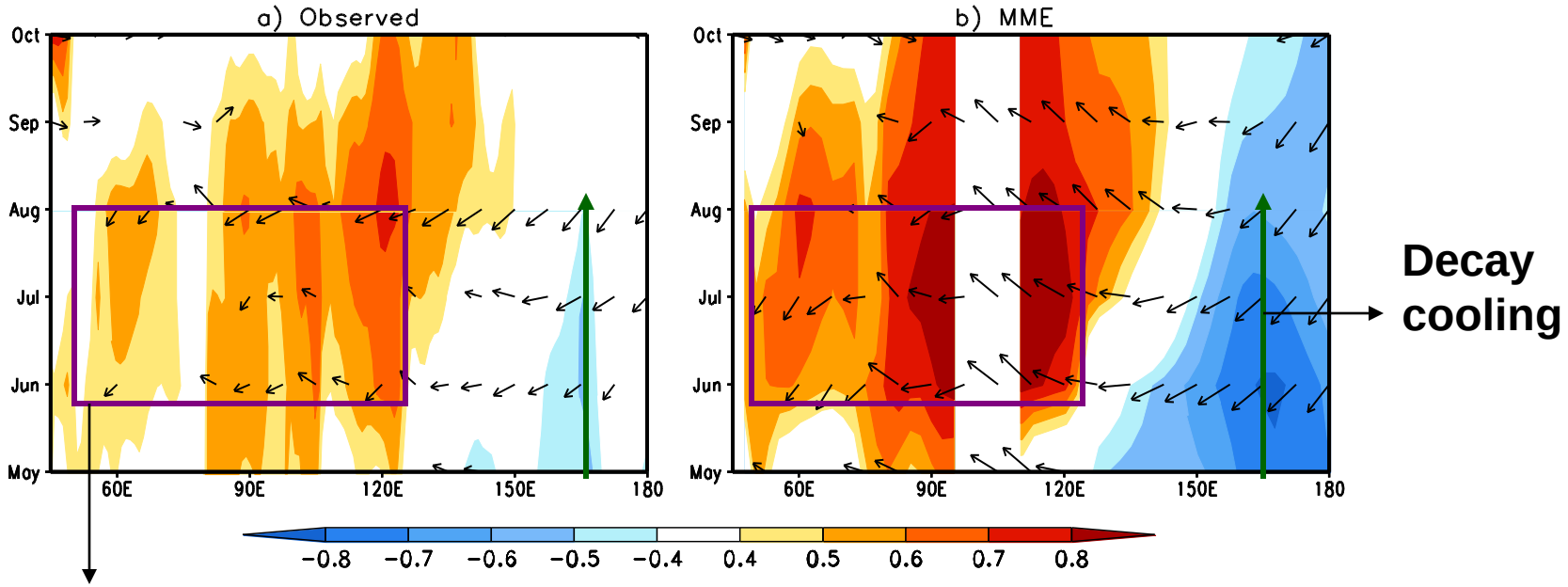

Correlation of SST (Shaded) and 850hPa wind anomalies (vectors) averaged from 5ºN to 20ºN against the NW Pacific SLP PC-1: (a) observations, (b) MME initialized on 01May. Y-axis is calendar month during decay phase of El Niño.

Composites of summer following El Niño

Strengthened westerly jet and rainfall

SST (shaded;°C), SLP (contours; hPa) and 850hPa wind anomalies

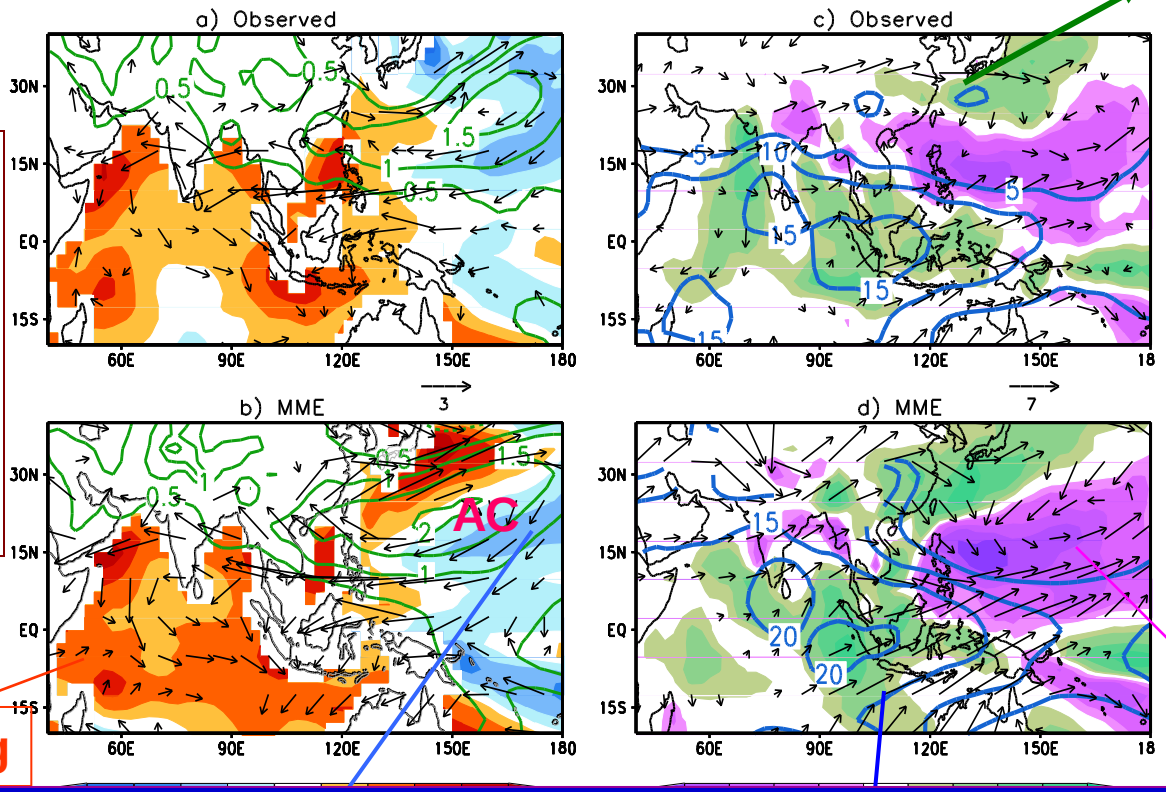

Precipitation (shaded) TT (contours), and 200hPa wind anomalies winds (vectors).

TIO warming

Suppressed rainfall

3. The subtropical westerly jet intensifies on the northern flank of the TT warming induced by the positive SST anomalies over the TIO. The intensified westerly jet could enhance atmospheric convection over the Meiyu/Baiu rain band by advecting warm temperature from the Tibetan plateau region (Sampe and Xie 2010). A surface circulation in response to enhanced Meiyu/Baiu convection would induce surface wind divergence in the subtropics and suppress convection there (Chowdary et al., 2010, submitted).

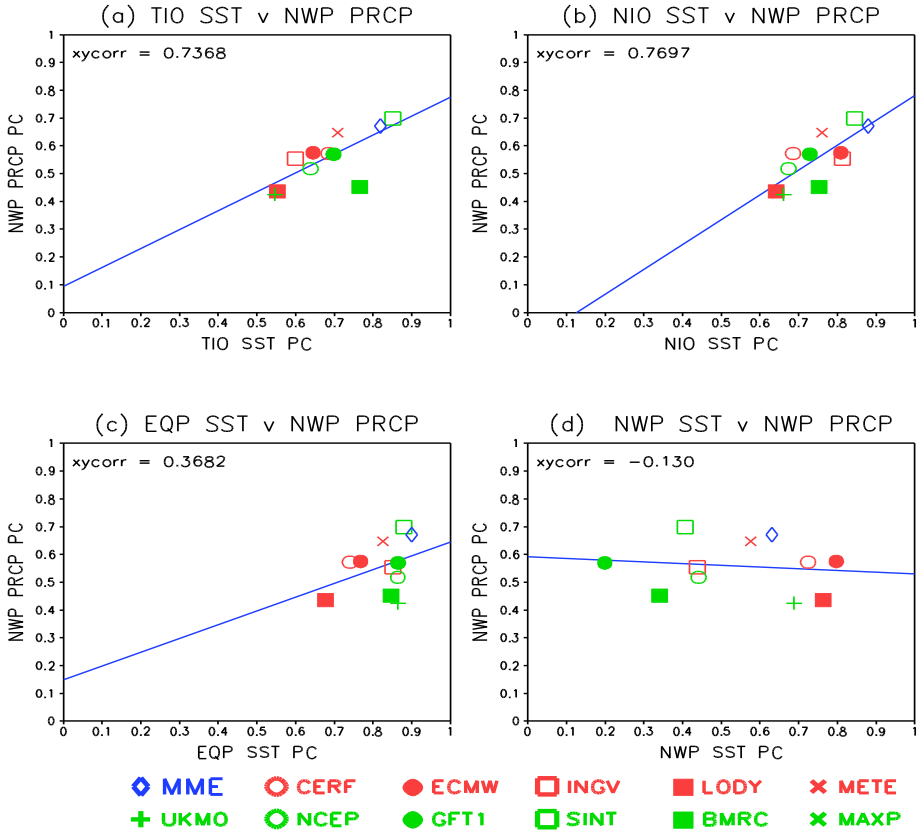

Scatter diagram between the forecast skill of JJA NW Pacific precipitation PC-2 and skills of regional SST PCs

(a) the TIO (20ºS-20ºN and 45ºE-100ºE)
(b) the NIO SST (0-20ºN and 45ºE-100ºE)
(c) the equatorial Pacific (20ºS-20ºN and 120ºE-90ºW)
(d) the NW Pacific (0-40ºN and 120ºE-160ºE). All based on one-month lead forecast.

Strong correlation in skills between SST anomalies over TIO/NIO and NW Pacific rainfall predictability. Models that are skilful in capturing TIO/NIO SST anomalies are likely to be successful in predicting NW Pacific rainfall variability.

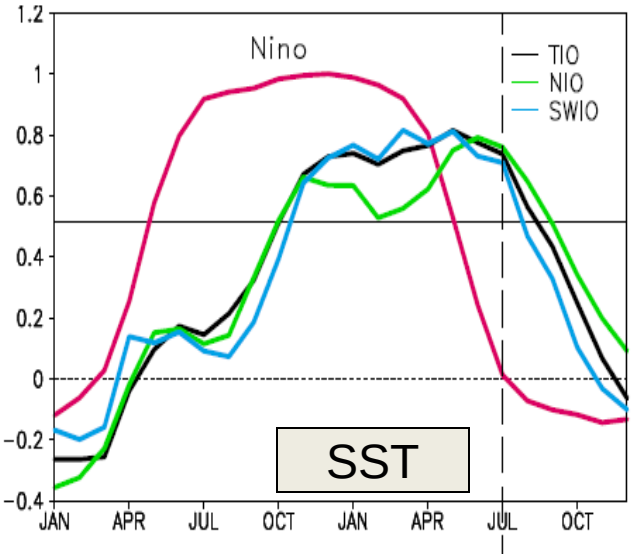

Nino 3.4 Correlation with TIO; NIO and SWIO SST anomalies (Du et al., 2009; Xie et al., 2010)

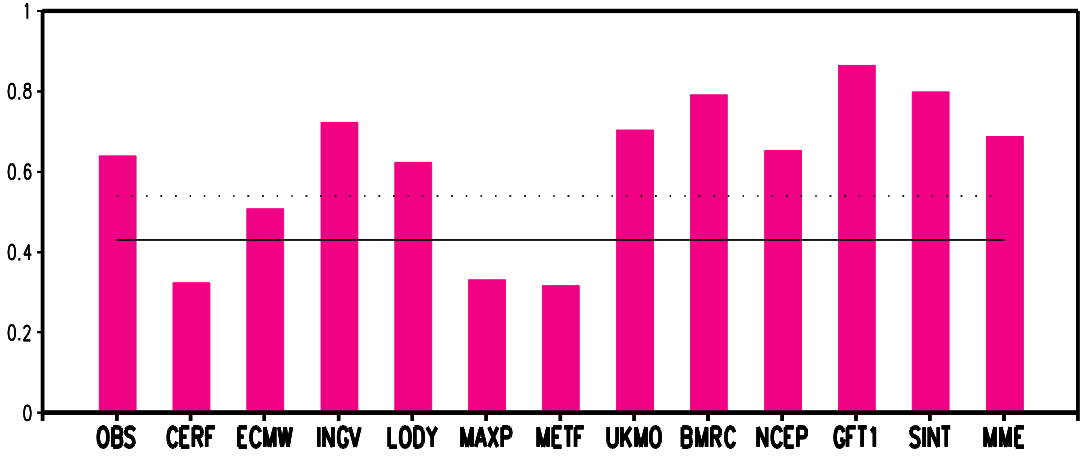

Correlation coefficient between summer NIO SST PC and NW Pacific at four-month lead. (here summer refers to June and July).

✓Correlation is 0.64 for observations and 0.68 for the MME four-month lead prediction (here summer refers to June and July).

✓Some models underestimate the relationship between NIO SST and NW Pacific precipitation compared to observations (e.g; MAXP and METF).

Solid and dotted lines represent 95% and 99% confident levels, respectively.

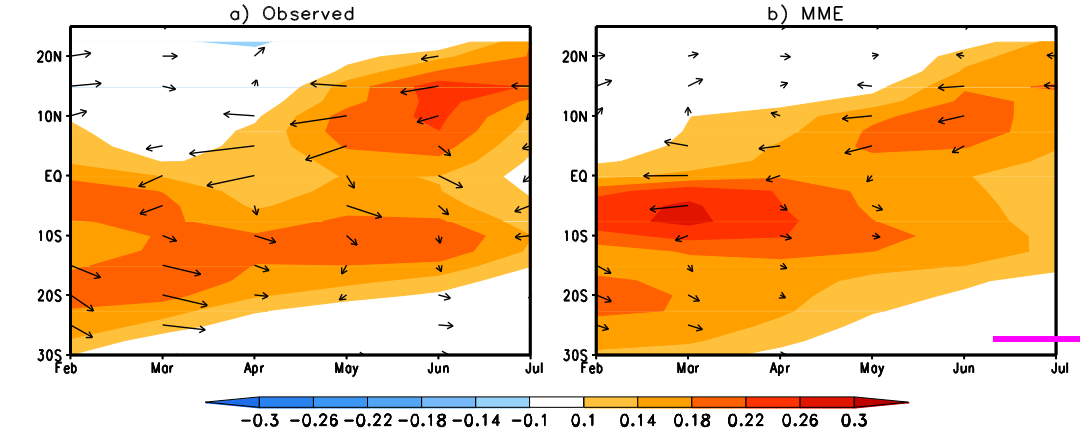

Regression of SST (Shaded; ºC) and 850hPa wind anomalies (vectors; m/s) averaged zonally in 40ºE to 100ºE against the observed NDJ(0) Niño-3.4 SST index: (a) observations and (b) MME initialized on 01February.

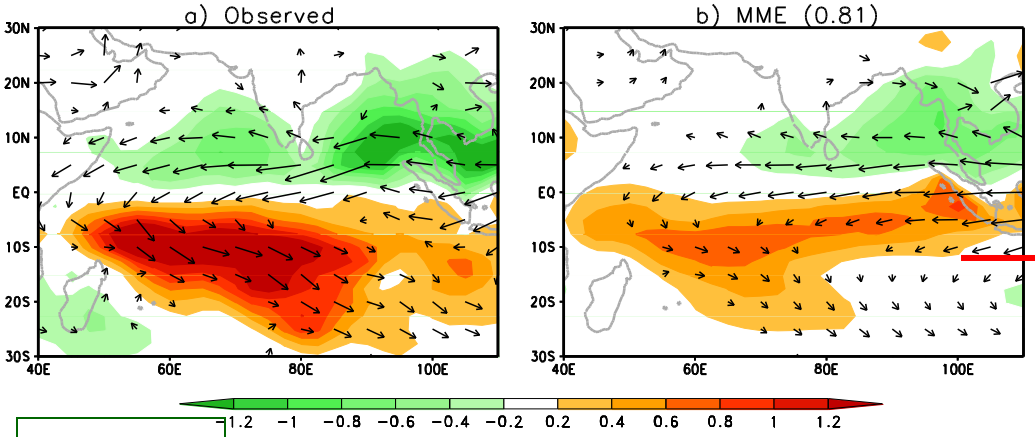

MAM rainfall EOF-1 over the TIO for observations and one-month lead model prediction (initialized from 01February) .

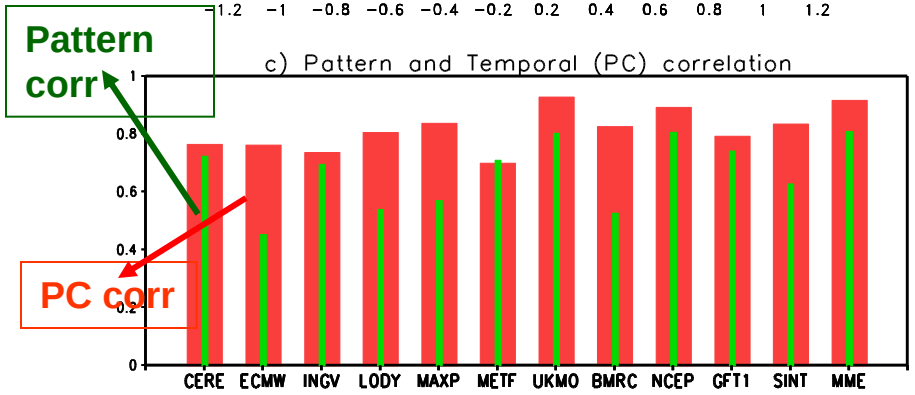

Models are successful in predicting the anti-symmetric patterns of precipitation and winds over TIO during spring, which are critical to sustaining the TIO warming through the subsequent summer.

Summary:

✓**Analysis of multi-model hindcasts demonstrated that to predict NW Pacific atmospheric anomalies during JJA(1), our result show that models need to predict the TIO SST and precipitation well along with SST cooling on the south-eastern flank of anticyclone.**

✓**Two mechanisms are identified for TIO to affect NW Pacific rainfall variability during JJA(1) remotely. One is the Kelvin wave- induced Ekman divergence mechanism [*Xie et al*., 2009] and the other is through intensifying the subtropical westerly jet.**

✓**This study also showed that most models are successful in predicting the anti-symmetric patterns of precipitation and winds over TIO during spring as they are essential to maintaining the TIO warming through the subsequent summer.**

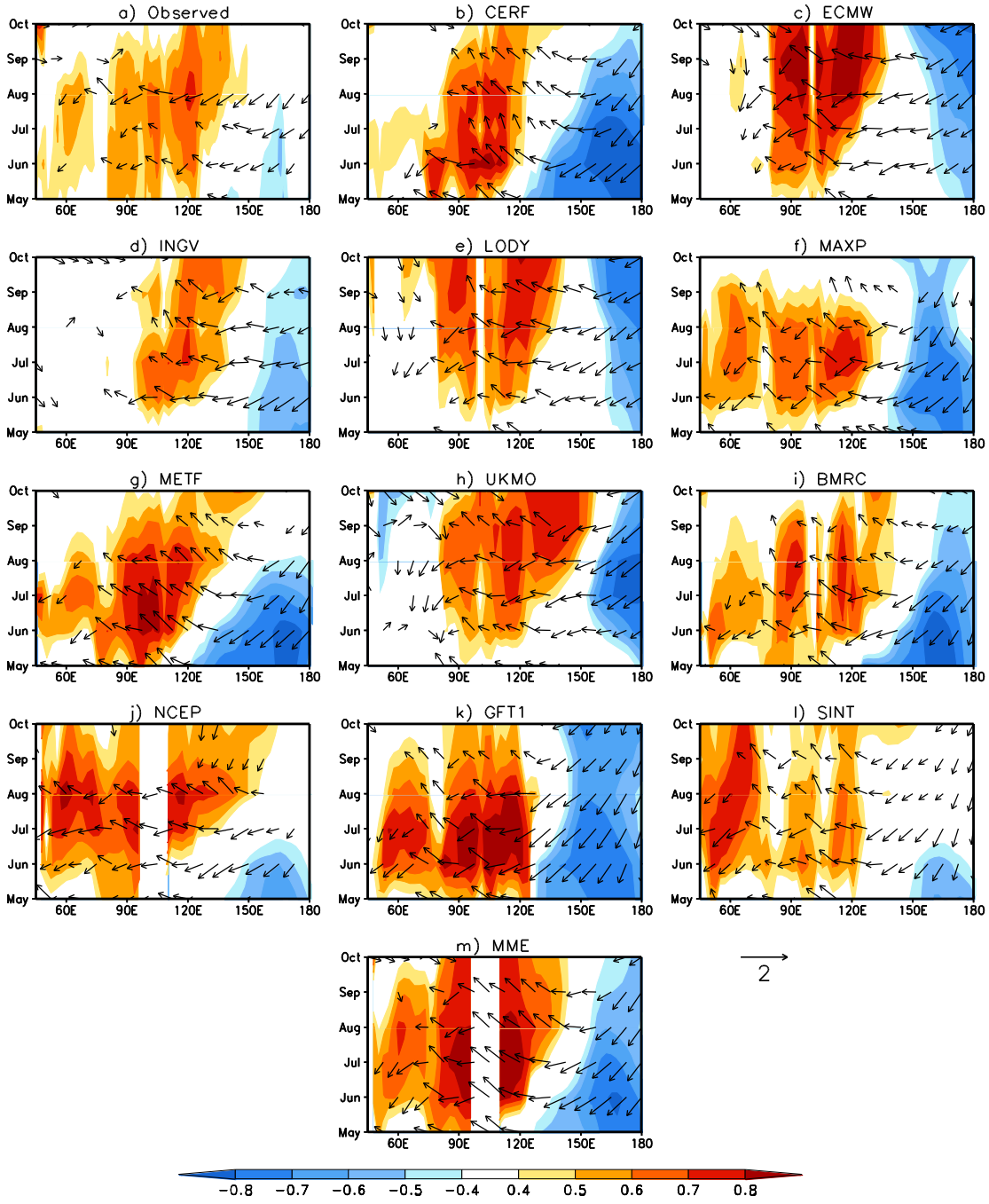

Figure: Correlation of SST (Shaded; ºC) and 850hPa wind anomalies (vectors; m/s) averaged from 5ºN to 20ºN against the NW Pacific SLP PC-1: (a) observations, (b)-(l) individual models, and (m) MME initialized on 01May. Y-axis is calendar month during decay phase of El Niño.

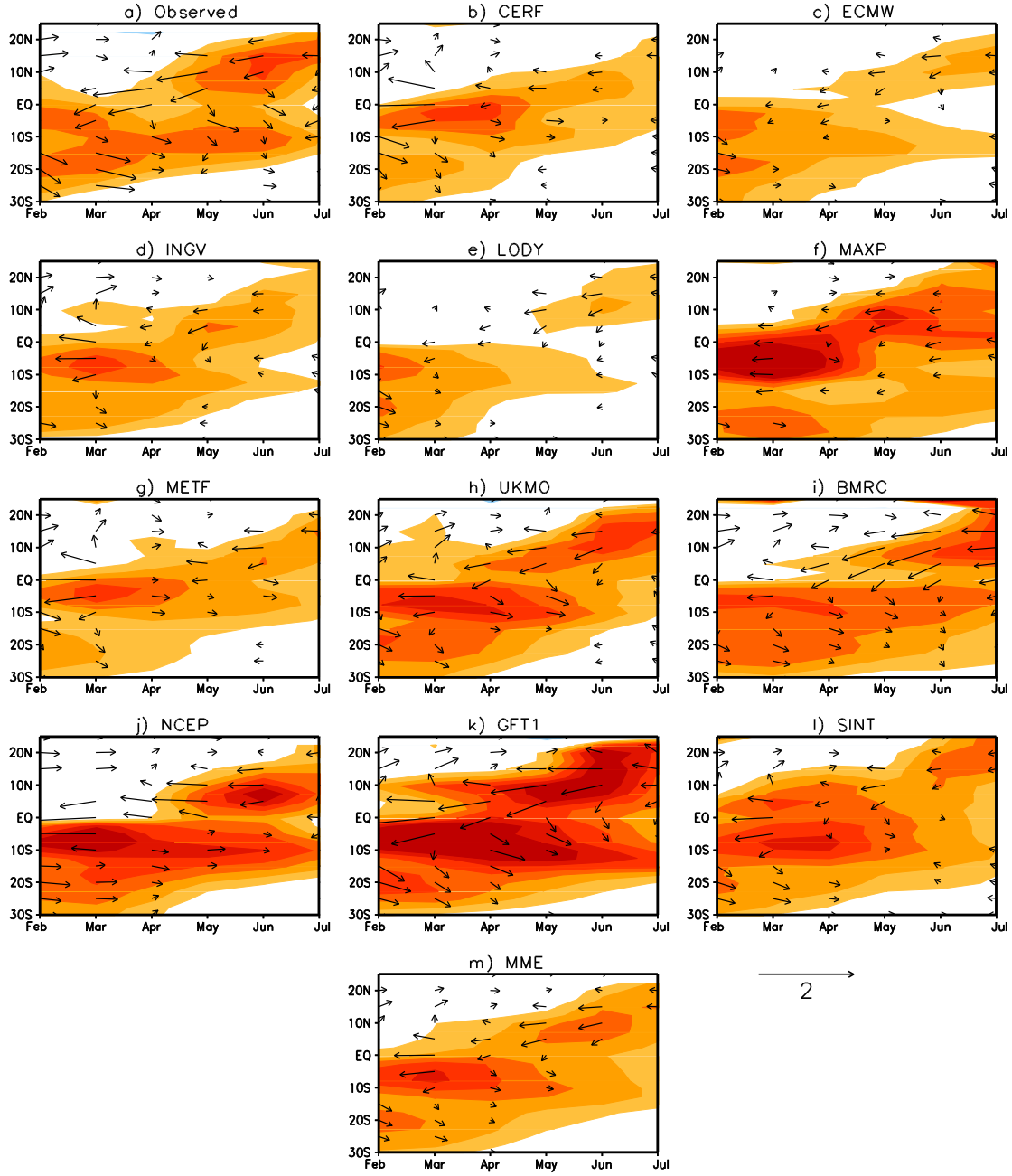

Figure: Regression of SST (Shaded; ºC) and 850hPa wind anomalies (vectors; m/s) averaged zonally in 40ºE to 100ºE against the observed NDJ(0) Niño-3.4 SST index: (a) observations, (b)-(i) individual models, and (m) MME initialized on 01February.

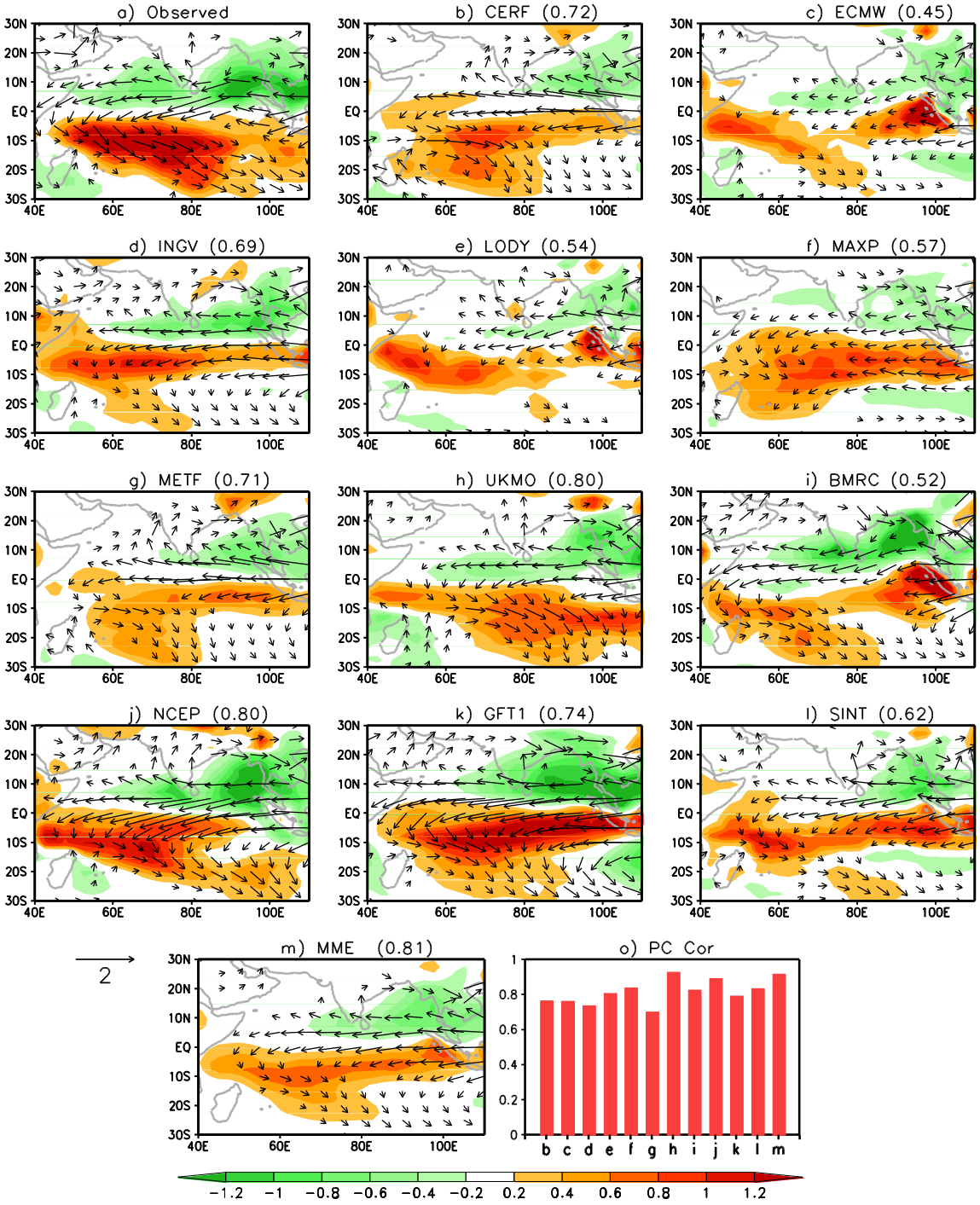

Figure:. The first EOF of (MAM) precipitation (shaded) variability (a) observations, (b)-(i) models, (m) MME 1-month lead prediction. (o) Temporal correlation for precipitation PCs between models and observations over the TIO. Vectors represent the 850hPa wind anomalies (m/s) regressed upon corresponding rainfall PC (a - m). The pattern correlation between the observed and predicted EOFs is shown at the top of each panel (b-m).

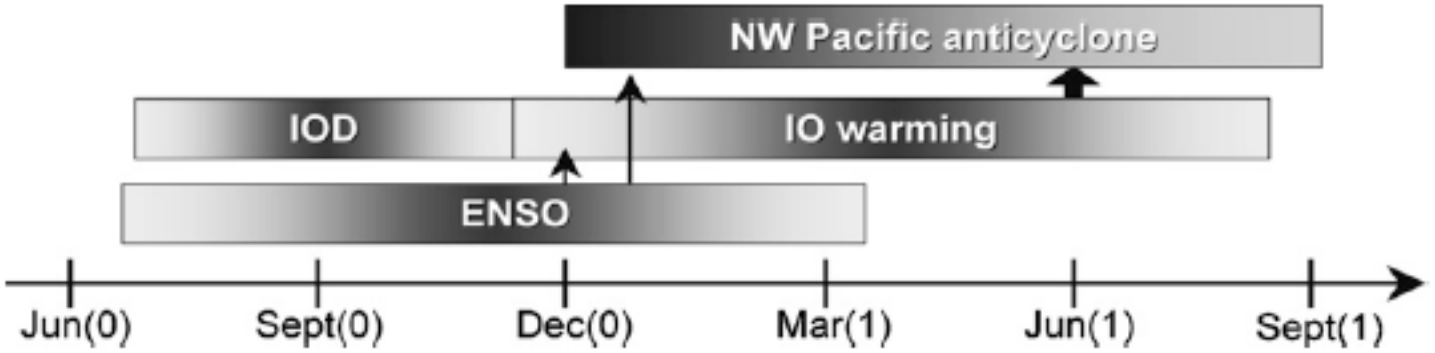

FIG. 13. Seasonality of major modes of Indo–western Pacific climate variability. Vertical arrows indicate causality, and the block arrow emphasizes the TIO capacitor effect, the major finding of the present study.

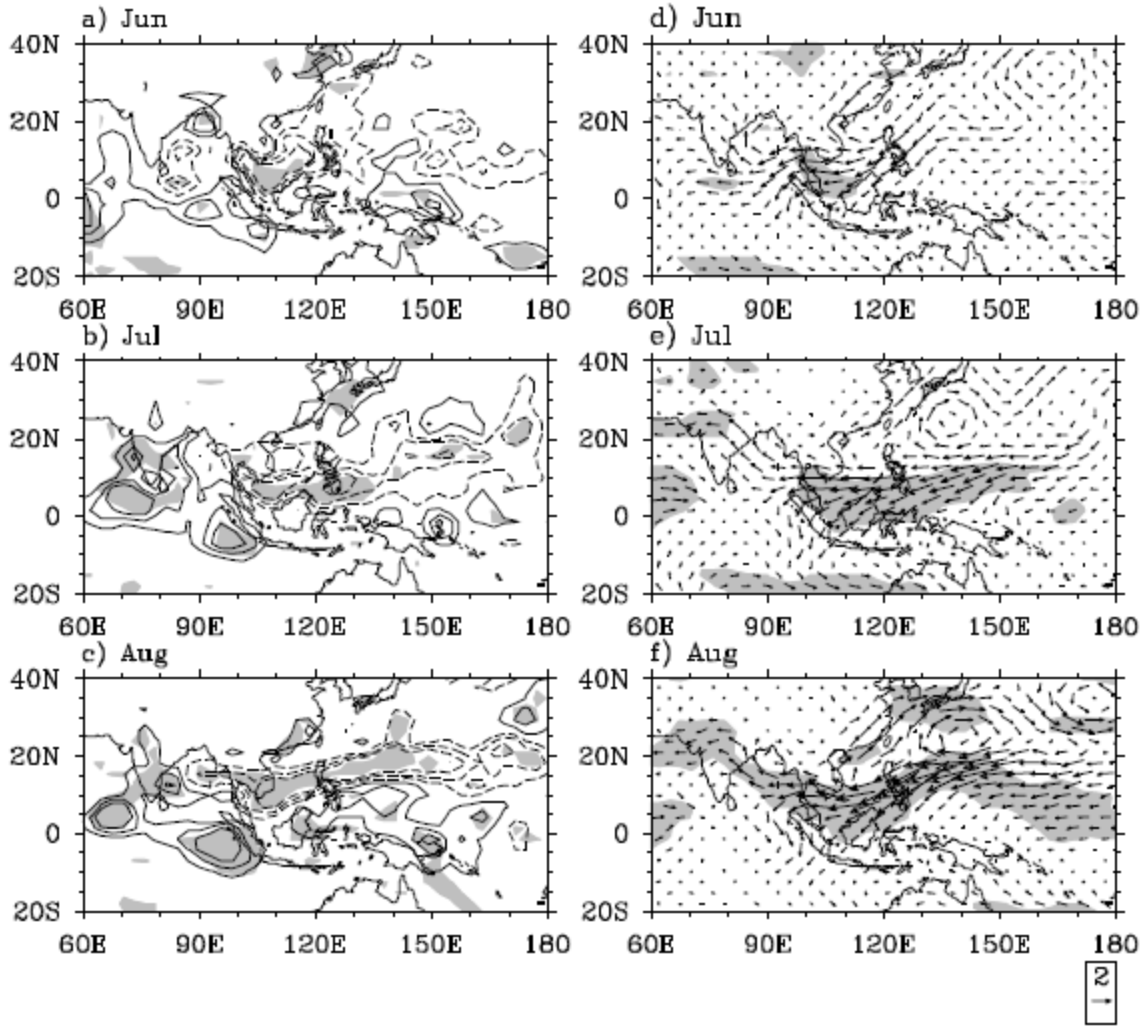

Fig. 9 Same as Fig. 6, except for the difference between TIO and CTRL runs.

Fig. 6 Difference of the precipitation (left panel, units: mm/day) and 850hPa wind (right panel, units: m/s) between the GB and CTRL runs. The contour values at left panel are ±1, ±2.5, ±4. Solid (dashed) lines denote positive (negative) values. The shading represents the 5% significant level for the precipitation (left panel) and the zonal wind (right panel). ECHAM4 CTRL run

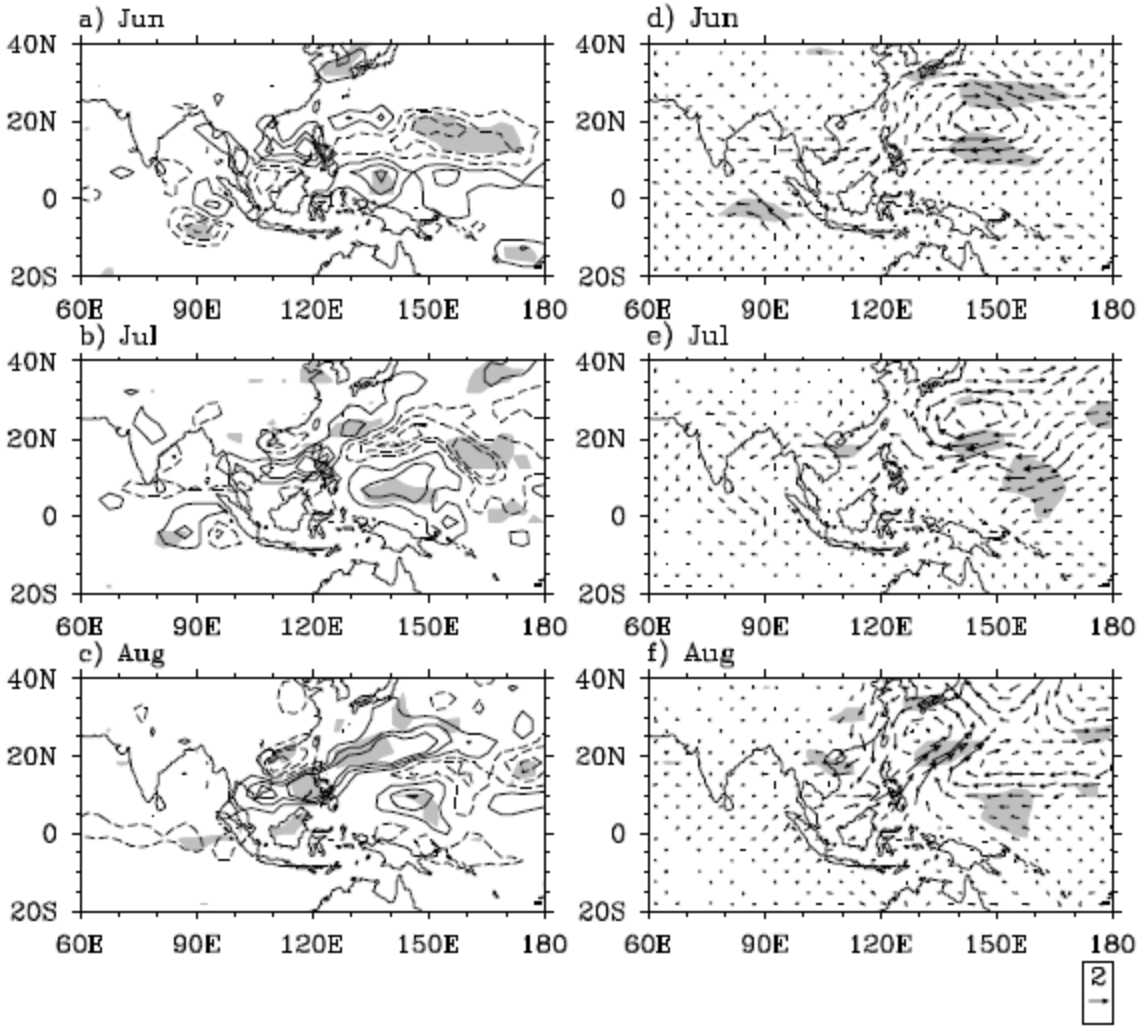

Fig. 8 Same as Fig. 6, except for the difference between the WNP and CTRL runs.

With the aid of a set of numerical experiments Wu et al (2010) demonstrate that both the negative SSTA in the NW Pacific and the TIO Basin-Mode contribute to the maintenance of the NW Pacific anticyclonic circulation in summer following El Nino.

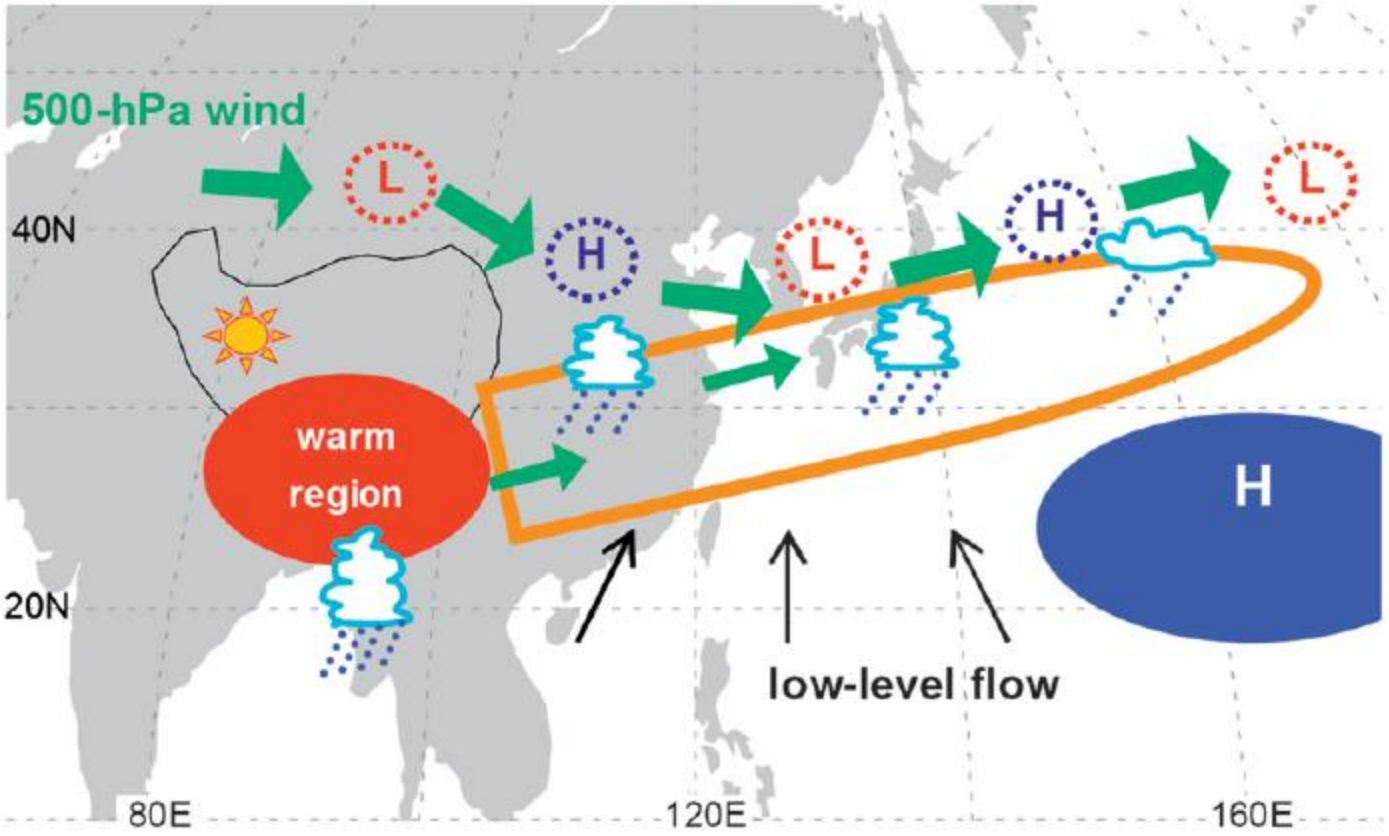
500-hPa wind
40N
20N
80E
120E
160E
L
H
L
H
L
warm
region
H
low-level flow

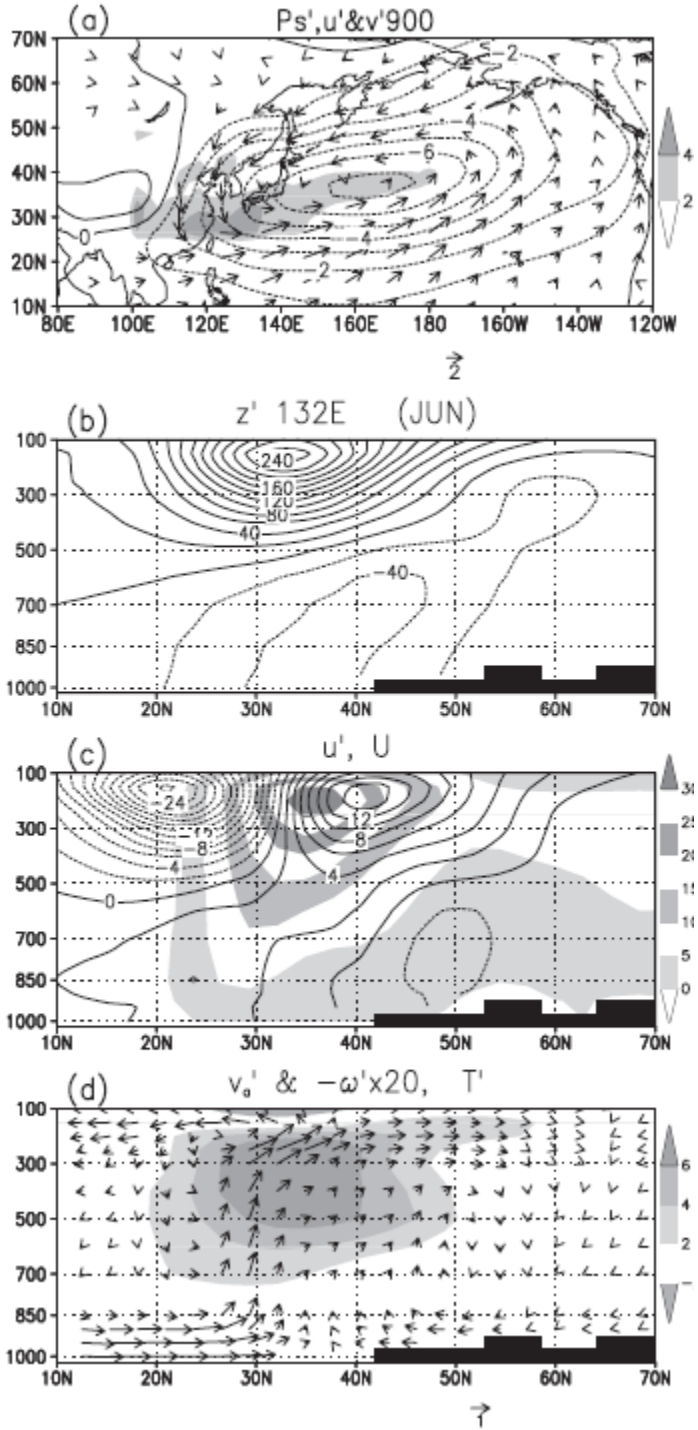

FIG. A1. LBM response to June heating of JRA-25 prescribed in the domain (258–508N, 1008E–1608W). (a) Surface pressure (contours at every 1 hPa), 900-hPa wind (arrows) and the prescribed heating at the 0.45 sigma level (shading, K day21). Meridional sections at 1328E: (b) geopotential height (contours at every 20 m); (c) zonal wind velocity (contours at every 2 m s21) overlaid on the basic-state zonal wind velocity (shading, m s21); (d) temperature (shading in K) with meridional and vertical components of ageostrophic wind (arrows in m s21 and Pa s21, respectively; vertical component is multiplied by 20).

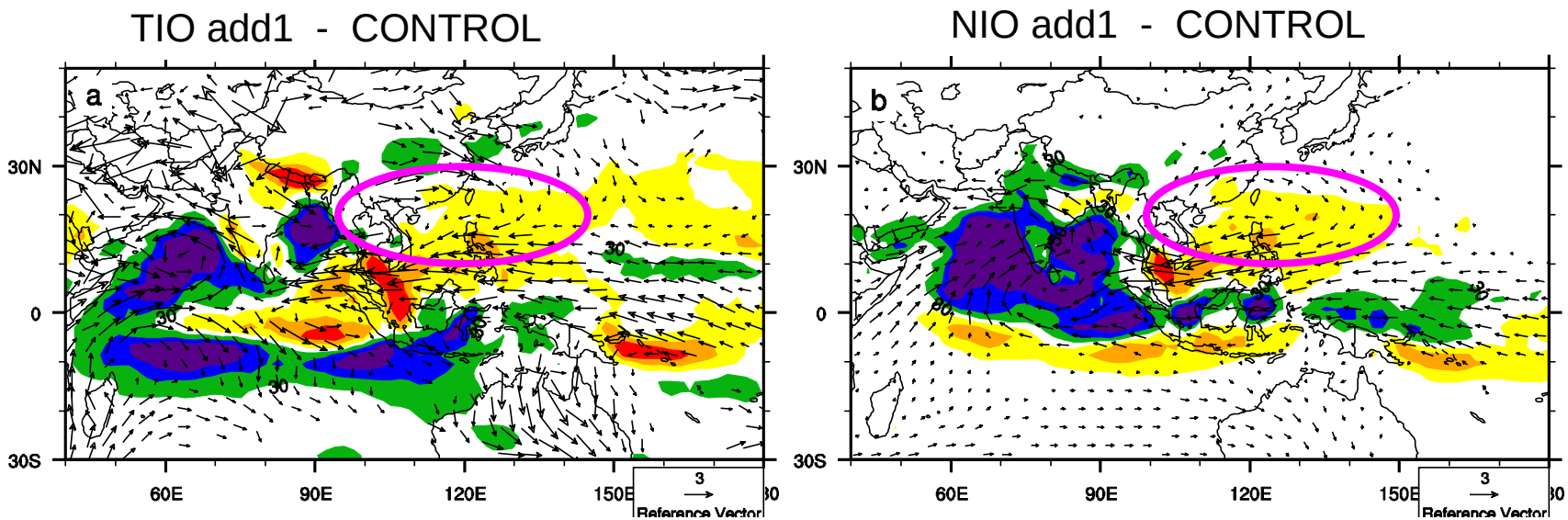

FIG Difference of mean summer precipitation (color-shaded) and 850hpa wind (a) between all tropical Indian Ocean SST add1k experiment and climatological SST experiment; (b) between north tropical Indian Ocean SST add 1k experiment and climate SST experiment; (the wind field was showed in the area where significant at 95f% confidence level) (ECHAM5.3 IOC)

Huang et al (2010) J.Clim